Science of the Total Environment 912 (2024) 168800

Contents lists available at ScienceDirect

Science of the Total Environment

journal homepage: www.elsevier.com/locate/scitotenv

A novel tool for tracing water sources of streamflow in a mixed land-use catchment

Zhi-Xiang Sun [a,b], Jun-Fang Cui [a,*], Jian-Hua Cheng [c], Xiang-Yu Tang [c,**]

[a] Institute of Mountain Hazards and Environment, Chinese Academy of Sciences, Chengdu 610041, China
[b] University of Chinese Academy of Sciences, Beijing 100049, China
[c] State Key Laboratory of Subtropical Silviculture, Zhejiang A&F University, Hangzhou 311300, China

HIGHLIGHTS

- Fluorescence ratio of two humic DOM components is proposed as water source tracer.
- Water source separation of streamflow in a mixed land-use catchment was conducted.
- The applicability of the fluorescence tracer was validated by water O-18 in forest.
- The fluorescence tracer can identify more than two pre-event water sources.

GRAPHICAL ABSTRACT

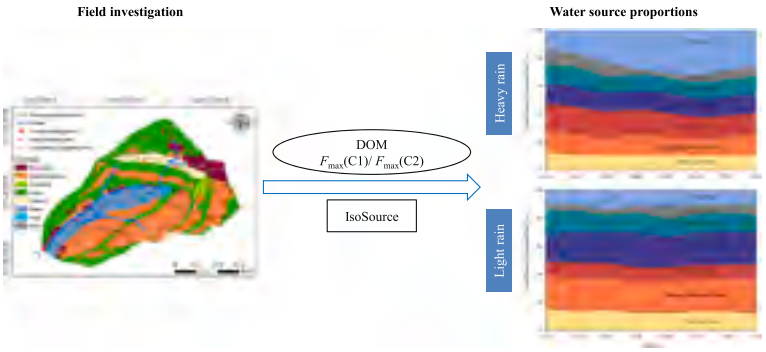

ARTICLE INFO

Editor: Jurgen Mahlknecht

Keywords:
Dissolve organic matter
Fluorescence
Water source
Tracer
Catchment
Land-use

ABSTRACT

Tracing water sources of streamflow in a mixed land-use catchment is critical for predicting pollutant emissions from various human activities to streams but remains a major challenge. A rain event based field monitoring study was conducted in the Jieliu catchment located in the hilly area of central Sichuan Province, southwest China. The ratio of the maximum fluorescence intensities (F_{max}) of the two humic-like dissolved organic matter (DOM) components at excitation/emission wavelengths of 255 (315)/415 nm (component 1; C1) and 260 (375)/480 nm (component 2; C2) was proposed as a tracer for quantifying streamflow water sources. Satisfactory performance of using the F_{max}(C1)/F_{max}(C2) ratio in hydrograph separation of streamflow at the outlet of a forest sub-catchment was verified by through comparison with the hydrograph separation results based on $\delta^{18}O$ data. The F_{max}(C1)/F_{max}(C2) ratio was then applied to estimate the contributions of rainwater and pre-event water sources under different land use types to the streamflow in an agro-forest sub-catchment and the entire catchment. The hydrograph separation results using the F_{max}(C1)/F_{max}(C2) ratio can be used to support the optimization of water resource management and the quantification of pollutant loadings from major water sources to streams at the catchment scale.

* Corresponding author.
** Correspondence to: X.-Y. Tang, State Key Laboratory of Subtropical Silviculture, Zhejiang A&F University, Hangzhou 311300, China.
E-mail addresses: jfcui@imde.ac.cn (J.-F. Cui), xiangyu.tang@foxmail.com (X.-Y. Tang).

https://doi.org/10.1016/j.scitotenv.2023.168800
Received 16 September 2023; Received in revised form 29 October 2023; Accepted 20 November 2023
Available online 27 November 2023

1. Introduction

Water source identification of streamflow in a mixed land use catchment is of utmost importance for optimizing the management of the quantity and quality of rivers but remains difficult. Water isotopes (e.g., ^{2}H and ^{18}O) are the most commonly used conservative tracers to distinguish event (e.g., rainfall) water from pre-event water. However, they do not have very high specificity (i.e., different pre-event water sources can have the same isotopic ratio). The poor specificity of isotopic signature in various pre-event water sources precludes the use of water isotopes to estimate the water contributions of different land uses to streamflow in a catchment during a rain event (Abbott et al., 2016).

A variety of solutes, including natural ions (e.g., Cl^{-}, NO_3^{-}, SO_4^{2-}, Na^{+}, and Ca^{2+}), artificial sweeteners (e.g., acesulfame and sucralose), and pharmaceuticals (e.g., carbamazepine, sulfamethoxazole, diclofenac, and caffeine), have been used as environmental tracers to identify water sources (Abbott et al., 2016; Buerge et al., 2009; Lubick, 2009; Riml et al., 2013). The concentrations of some natural cations and anions often differ between rainwater, groundwater, and soil water because of various biogeochemical processes. Therefore, they can be selected to estimate the contributions of pre-event water sources (e.g., soil water and groundwater) to streamflow during rainfall (Stewart et al., 2022; Xiao et al., 2023). Nevertheless, the applicability of natural ions for identifying water sources from different land uses remains unclear because their specificity has not been extensively evaluated. Anthropogenic pollutant tracers can be used to track contaminated water sources; however, their applications are mostly limited to small temporal and spatial scales owing to their reactivity in the environments (Abbott et al., 2016; Buerge et al., 2003).

Dissolved organic matter (DOM) is a biogenic tracer that may be more versatile than other solutes for tracking water from multiple sources. DOM is ubiquitous in various environmental media (such as precipitation, soils, water bodies, and wastewater). In particular, the inherent quality of plant material and land use directly control the chemical composition of DOM (Cotrufo et al., 2022; Zhao et al., 2020). As a mixture of thousands of dissolved carbon compounds, DOM may have distinct properties (e.g., chemical composition, isotopic signature, optical properties, and stoichiometry). DOM is often assumed to be conservative; thus either a single or multiple properties of DOM can be used to identify water source(s) and flow path(s) (Begum et al., 2023; Ramón et al., 2021; Voss et al., 2015).

Different water sources may have the same dissolved organic matter (DOC) concentration but different compositions, resulting from various biogeochemical processes or human activities. Although fluorescent compounds account for only a small portion of the total DOM pool (Fellman et al., 2010), the conservative components of DOM have potential as tracers for distinguishing water sources. Protein-like fluorescent compounds (e.g., tryptophan and tyrosine) are the most degradable components of DOM in the environment (Cory and Kaplan, 2012). The contribution of protein-like compounds to DOC concentration could lead to a decrease in the ability of DOC concentration to trace streamflow water sources. Our previous study found that the ratio of the maximum fluorescence intensities of two humic-like components was as conservative as ^{18}O during the mixing of rainwater and pre-event soil water on sloping farmland and thus may serve as a water tracer for hydrological paths at the plot scale (Xian et al., 2018). Fluorescent DOM has also been used to trace temporal changes in hillslope-to-stream connectivity and to track the interactions between surface water and groundwater (Burns et al., 2016; Hu et al., 2016; Quiers et al., 2013). Therefore, we assumed that humic-like DOM components in potential pre-event water sources were stable at the rain-event scale and experience conservative mixing during rainfall-induced hydrological processes at a small catchment scale. Moreover, the abundance ratio of the two conservative DOM components should have a higher specificity than their DOC concentration-normalized abundances. To the best of our knowledge, no multiple scale field investigations have been reported on the use of the abundance ratio of two stable fluorescent DOM components to estimate the contributions of water from different land uses/vegetation covers to streamflow at the catchment scale.

The objective of this study was to evaluate the feasibility of using the ratio of the maximum fluorescence intensities of two conservative DOM components to quantitatively distinguish between the contributions of rainwater and multiple pre-event water sources to streamflow in a mixed land-use catchment. The results of this field study offer a novel tool that can be used to support the optimization of water resource management and the protection of major streamflow water sources from pollution by anthropogenic activities.

2. Materials and methods

2.1. Site description

The study area (31°16′ N, 105°28′ E) is a small headwater catchment (35 ha; Jieliu catchment) located in Yanting, Sichuan, Southwest China (Fig. 1). The catchment elevation ranges from 405 to 535 m above sea level (a.s.l.). This area features a moderate subtropical monsoon climate, with the annual average temperature and rainfall (1981 to 2006) being 17.3 °C and 826 mm, respectively. In total, 5.9 %, 65.5 %, 19.7 %, and 8.9 % of the annual precipitation is distributed in the spring, summer, autumn and winter, respectively (Zhao et al., 2013a). The dominant land use type in the Jieliu catchment is sloping farmland, which accounts for 42.2 % of its total area and is planted with maize and corn in rotation. Other main land use types included forests (32.2 %), paddy fields (9.9 %), residential areas (7.6 %), orchards (5.2 %) and grasslands (1.7 %). The forestlands were alder-cypress mixed plantations whereas the orchards in the middle catchment were mainly planted with lemon trees. The slopes of the catchment are dominated by purple soil, which is loamy and classified as an Entisol according to the soil taxonomy of the United States Department of Agriculture. The valley area of the catchment is dominated by paddy soils.

On slopes, rainwater largely travels through the thin soil layer (normally <60 cm, and particularly <50 cm on steep forestland) via preferential flow as well as piston flow, then quickly passes through the fractures in the mudrock and finally flows laterally over the top of the impermeable sandstone layer underneath the mudrock into the streams (Zhao et al., 2013a). Paddy fields have a low-permeability soil layer at a depth of 45–50 cm (Liu et al., 2022), above which lateral flows may occur. Therefore, in this study, the top 50 cm of the soil layer was considered the major source of soil water contributing to the streamflow. Stream water flows from the northeast to southeast of the catchment. There are six wells in the catchment area. Five wells were constructed in a flat valley and were used mainly as sources of drinking water for local farmers. Another well with no human perturbations was located on the lower slope east of the pond. The shallow groundwater levels in the six wells varied in the ranges of 411–431 m a.s.l. in August 2021, and 410–431 m a.s.l. in June 2022. The lowest groundwater levels were observed in the well nearest the catchment outlet, while the highest groundwater levels were detected in the well on the lower slope. In this catchment, shallow groundwater is available only in the lowland areas and no groundwater was found in the highland areas (Zhang et al., 2019). Sloping farmlands are rain-fed, while paddy fields are sometimes irrigated for rice growth with water pumped from wells in the valley during dry days (Zhang, 2015).

2.2. Sampling and analysis

Sampling campaigns for rainfall, soil waters (including total and mobile soil water) under different land uses, residential runoff (a mixture of rainwater, overland flow, and domestic wastewater collected by the sewerage system), streamflow, and shallow groundwater (well water) were conducted in the Jieliu catchment.

Two representative lands of each of the five vegetation cover types

(forest, orchard, grassland, sloping farmland, and paddy fields) in the catchment were selected (Fig. 1). Suction cup soil water samplers (1900, Soil Moisture Equipment Corp., Santa Barbara, CA, USA) were installed at depths of 5–10, 15–20, 25–30 and 45–50 cm to collect mobile soil water before and after rainfall by applying a maximum tension of −80 kPa with a vacuum. On the other hand, right before and after rainfall, disturbed soil samples were collected with core sampler (50 mm inner diameter) from the same four depths at three sampling points, and three samples from the same depth were combined to form a composite sample. Undisturbed soil cores (100 cm^3) were also taken in triplicate.

Owing to difficulties and constraints encountered in the field, only two successful sampling/monitoring campaigns were conducted during the summers of 2021 and 2022. Two complete sets of hydro-climatic data and samples of various types were obtained at all locations for the rain events on August 22, 2021, and June 26, 2022. The rain event on August 22, 2021, had a higher amount and a greater maximum intensity than the rain event on June 26, 2022, and was thus defined as a "heavy rain" in this paper for convenience. Accordingly, the rain event on June 26, 2022 was referred to as a "light rain" hereinafter. Before each rain event, the residential runoff samples were collected at the outlet of residential sub-catchment, and groundwater samples were collected from six wells (Fig. 1). Although all six wells are located in forest areas, they can be recharged not only by forest drainage but also by subsurface flows from potential source areas under different land uses/vegetation covers (Zhao et al., 2013a). Therefore, groundwater samples collected from these wells were used to represent groundwater in the catchment. At the outlets of the Jieliu catchment (S_{JL}) and its forest (1.6 ha; S_F), residential (2.02 ha; S_R) and agro-forest (12.1 ha; S_{AF}) sub-catchments, streamflow/runoff samples were collected at 30-min intervals during rainfall. For each rain event, rainwater samples were collected near all soil sampling locations in 1-l containers until the rain stopped. A funnel was connected to each container and a table tennis ball was placed in the funnel to reduce evaporation. In addition, it should be noted that 2022 (annual rainfall: 581.1 mm; annual average temperature: 17.2 °C) was a much drier and slightly warmer year than 2021 (annual rainfall: 1389.2 mm; annual average temperature: 16.4 °C). Stream discharge was monitored every 15 min with a float-type (Huazheng, Chongqing, China)/capacitance-type (Odyssey, Christchurch, New Zealand) water level meter using a calibration relationship between the water flux and level.

Total soil water, which includes both matric-bound stationary water and mobile water in soil (Landon et al., 1999), was extracted using a cryogenic vacuum distillation system having four extraction units (West et al., 2006). Each unit consists of extraction and collection tubes. A sample vial containing the soil sample was placed in an extraction tube in a heating cup. All the five units were connected to a vacuum pump. Water vapor emanating from the sample was trapped in a collection tube with liquid nitrogen. To ensure the complete extraction of water from the soil sample, extraction was conducted until no more water vapor appeared in the collection tube. Soil water collected with suction cup samplers represents the mobile fraction of water in the soil (Brooks et al., 2009). The bulk densities and volumetric water contents of the undisturbed soil core samples were measured.

Rainwater samples and all potential pre-event water samples were analyzed for $\delta^{18}O$ and DOM fluorescence. For isotopic analysis, water samples were filtered through 0.22 μm membrane filters into 2 mL glass vials with a cap containing a barrier and sealed with Parafilm® to prevent evaporation. The samples were stored in a refrigerator at 4 °C prior to analysis. Oxygen isotope analysis was performed using an L2120-i analyzer (Picarro, Santa Clara, CA, USA). The oxygen isotope data were expressed as $\delta^{18}O$, which is defined as the difference between the measured ratios ($^{18}O/^{16}O$) of the samples relative to the measured ratios of the Vienna Standard Mean Ocean Water (VSMOW) (Eq. (1)). The measurement precision for each sample was within 0.05 ‰.

$$\delta^{18}O_{\text{sample}} = \left(\frac{^{18}O/^{16}O_{\text{sample}}}{^{18}O/^{16}O_{\text{VSMOW}}} - 1\right) \times 1000‰ \quad (1)$$

Soil DOM was obtained by water-soil oscillation: the soil samples were extracted with ultrapure Milli-Q water at a soil/liquid ratio of 1/10 (*w/v*), shaken for 24 h at 180 rpm and 25 °C, and then filtered through 0.45 μm membrane filters. An Aqualog spectrophotometer (Horiba JY, Edison, NJ, USA) was used to analyze the fluorescence excitation-emission matrices (EEMs) of the water samples and water extracts of the soils. Excitation (Ex) and emission (Em) wavelength ranges were 250–500 and 200–600 nm, respectively. Milli-Q water was used as the blank to eliminate Raman scattering peaks. Rayleigh bands and Raman scattering in the EEM spectra are also removed. The fluorescent DOM components were identified by conducting parallel factor analysis (PARAFAC) using SOLO (Eigenvector Research Inc., Manson, WA, USA). Each component was quantified in terms of the maximum fluorescence

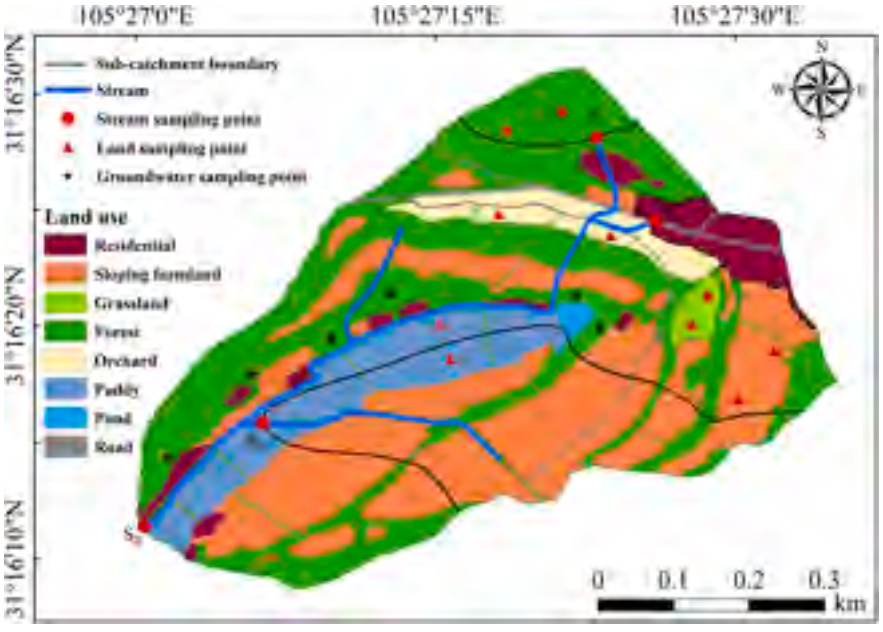

Fig. 1. Soil and water sampling locations in the Jieliu catchment located at Yanting, Sichuan, southwest China.

intensity (F_{max}), which was obtained by multiplying the fluorescent component loading by the maximum value of the corresponding excitation-emission spectral loading (Murphy et al., 2013).

2.3. Selection of tracers and end-members

Two humic-like fluorescent DOM components, component 1 (C1) and component 2 (C2), with peaks at Ex/Em wavelengths of 255 (315)/415 nm and 260 (375)/480 nm, respectively, were detected in all sources and streamflow samples (Fig. 2). Both C1 and C2 have complex structures that are difficult to degrade. They are highly conservative during mixing processes over short distances at the event scale (Abbott et al., 2016; Stedmon and Markager, 2003; Xue et al., 2022). In addition, although fluorescence in the region of protein-like components was detected in some water samples, it was too weak to be distinguished independently in most water samples. Given the relatively high biodegradability of protein-like component (Wickland et al., 2012), they were not considered tracers for water sources in this study. Therefore, the ratio of F_{max} of C1 and C2 was selected as a potential tracer to identify the water sources contributing to the streamflow.

The potentials of the total and mobile soil waters as end-member for tracing water sources were compared. Total soil water exhibited marked differences from groundwater in both F_{max}(C1)/F_{max}(C2) ratio and $\delta^{18}O$, whereas mobile soil water did not always differ from groundwater (Fig. S1). Moreover, it should be noted that mobile soil water samples were not always available at all four sampling depths, depending on the pre-event soil moisture. Therefore, the total soil water, rather than mobile soil water, was chosen to represent the pre-event water source for streamflow from the soil.

Pre-event end-member(s) from potential sources (total soil water with different vegetation covers, residential runoff, and groundwater) were selected based on the land-use composition and hydrologic connection of the water sources to the stream. In particular, groundwater was considered a potential end-member only for the catchment/sub-catchment with the outlet located at an elevation below the shallow groundwater table. Because the detected well water levels in the Jieliu catchment were at least 60 m below the outlet (485 m a.s.l.) of its forest sub-catchment, groundwater was not considered a potential end-member of the streamflow at S_F. Therefore, rainwater and forest soil water were selected as potential end-members of streamflow at the S_F during rainfall. The runoff baseflow at the outlet (457 m a.s.l.) of the residential sub-catchment was mainly domestic sewage and was considered a potential water source for the downstream area. For the agro-forest sub-catchment, rainwater, soil waters of forest, sloping farmland, paddy field, and groundwater were considered potential end-members of the streamflow at the outlet (414 m a.s.l.; S_{AF}) during rainfall. At the outlet (405 m a.s.l.; S_J) of the Jieliu catchment, rainwater, soil waters of forest, orchard, grassland, sloping farmland, and paddy field, residential runoff, and groundwater were considered potential end-members of the streamflow collected during rainfall.

Measurements of liquid water ^{18}O were used to validate the results obtained using the F_{max}(C1)/F_{max}(C1) ratio of DOM. The spatial variability of rainfall ^{18}O in the small Jieliu catchment was neglected. For each rain event, the mean values of F_{max}(C1)/F_{max}(C1) ratio and $\delta^{18}O$ for rainwater samples collected at all sampling locations were used to represent the tracer values of the event water end-member. The mean of the depth-averaged values of F_{max}(C1)/F_{max}(C2) ratio and $\delta^{18}O$ in total soil water collected prior to each rain event at the two representative

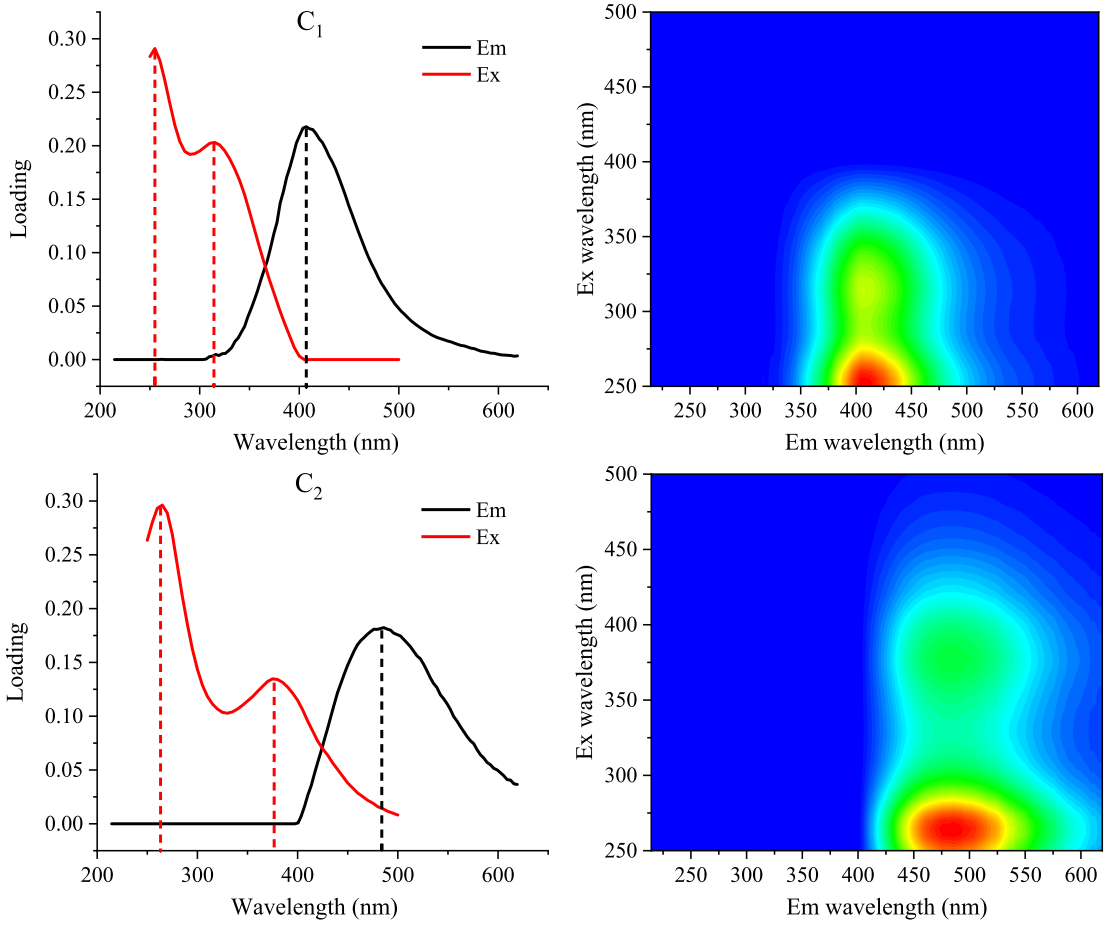

Fig. 2. The split-half validated results of excitation (Ex) and emission (Em) loadings of two major fluorescent DOM components (C1 and C2) identified using PARAFAC across all water source and streamflow samples. Corresponding contour plots of the same components are shown.

lands was used for each soil water end-member.

2.4. Hydrograph separation

To examine the capability of the new tracer $F_{max}(C1)/F_{max}(C2)$ ratio, the IsoSource model developed by Phillips and Gregg (2003) was employed to identify the plausibility of the potential water sources of the streamflow and their respective contributions, as it allows for the calculation of water contributions from more than two sources with a single tracer. The following mass balance equations were solved using an iterative algorithm:

$$\delta_Q = f_A\delta_A + f_B\delta_B + \ldots f_N\delta_N \quad (2)$$

$$1 = f_A + f_B + \ldots f_N \quad (3)$$

where Q is the discharge; δ is the tracer value; f is the fraction of each end-member; and the subscripts A, B and N refer to different end-members.

The IsoSource model was implemented with source increments of 1 % and a mass balance tolerance of ±0.5 ‰, which allows uncertainty derived from measurement error and sample variability of both sources and streamflow (Phillips and Gregg, 2001). The mean of the feasible contributions from each end-member was used as the final result, and the proportions of all end-members were summed to 100 %.

The IsoSource model was also used to estimate the contributions of rainwater and forest soil water to streamflow at the outlet of the forest sub-catchment (based $\delta^{18}O$ data to validate the new tracer) and the contributions of rainwater and pre-event total soil water to post-rain total soil waters under different vegetation covers (based on $F_{max}(C1)/F_{max}(C2)$ ratio and $\delta^{18}O$ data, respectively).

2.5. Evaluation of tracer performance

The performance of $F_{max}(C1)/F_{max}(C2)$ ratio in estimating water sources was evaluated by comparing it with the source proportion results determined by the traditional water isotope tracer ^{18}O in a single land-use drainage area of forest. In this study, the hydrograph separation results based on $\delta^{18}O$ data were considered as the true values (T_i), and the results by $F_{max}(C1)/F_{max}(C2)$ ratio were considered as the estimated values (E_i). The root mean square error (RMSE) and coefficient of determination (R^2) were calculated to evaluate the accuracy.

$$RMSE = \left[\frac{1}{n}\sum_{i=1}^{n}(E_i - T_i)^2\right]^{\frac{1}{2}} \quad (4)$$

$$R^2 = 1 - \frac{\sum_{i=1}^{n}(E_i - T_i)^2}{\sum_{i=1}^{n}(T_i - M_i)^2} \quad (5)$$

where n is the number of validation samples; E_i and T_i are the estimated and true value of the pre-event water's proportion in each streamflow sample, respectively; and M_i is the mean value of the pre-event water's true proportions in all streamflow samples during a rain event. Lower RMSE and higher R^2 indicate that the source proportion results have less errors and are more accurate.

2.6. Statistical analysis

Statistical analyses were conducted using SPSS software (version 20.0; SPSS Inc., Chicago, IL, USA). Differences in $F_{max}(C1)/F_{max}(C2)$ ratios and $\delta^{18}O$ values among different water sources (rainwater, total and mobile soil water, groundwater, and residential runoff) were analyzed using one-way analysis of variance (ANOVA). Differences in tracer values among the pre-event total soil waters of lands with different vegetation cover (forest, orchard, grassland, sloping farmland, and paddy) were also examined using one-way ANOVA. Relationships between $F_{max}(C1)/F_{max}(C2)$ ratio and $\delta^{18}O$ in each water source of streamflow were determined through linear regression analysis.

3. Results

3.1. Conservative fluorescent DOM components in water sources and streamflow

The excitation-emission spectral loadings of the two conservative fluorescent DOM components (C1 and C2) found in the samples of both the streamflow and its water sources are shown in Fig. 2. The C1 is similar to the C6 reported by Stedmon and Markager (2005), C2 by Williams et al. (2010), C2 by Hiriart-Baer et al. (2013), and C2 by Xian et al. (2018), which consisted of humic fluorophores of anthropogenic origin that are commonly present in aquatic and soil environments. The C2 identified in this study was similar to the C2 reported by Stedmon and Markager (2005), C3 by Kothawala et al. (2014), and C1 by Xian et al. (2018), which consisted of fulvic acid fluorophores of terrestrial or endogenous origin (mainly from soil microorganisms).

3.2. Differences in $F_{max}(C1)/F_{max}(C2)$ ratio and $\delta^{18}O$ among various water sources

The $F_{max}(C1)/F_{max}(C2)$ ratios of total and mobile soil water (data sets for all vegetation cover types are shown), groundwater, and residential runoff prior to rainfall were significantly different from those of rainwater on both August 22, 2021, and June 26, 2022 (Fig. S1). For the 2021 rain event, the differences in $F_{max}(C1)/F_{max}(C2)$ ratio were significant among the total soil water, residential runoff and groundwater; however the difference was insignificant between mobile soil water, and groundwater. In contrast, for the 2022 rain event, significant differences were observed between all four pre-event water source types. The lowest mean values of $F_{max}(C1)/F_{max}(C2)$ ratios were detected in the rainwater for both events. It appears that under hydro-climatic conditions $F_{max}(C1)/F_{max}(C2)$ ratios in mobile soil water, groundwater, and residential runoff are more variable than total soil water. In particular, higher $F_{max}(C1)/F_{max}(C2)$ ratios (i.e., greater relative abundance of humic fluorophores) in pre-event groundwater were observed in drier and warmer conditions in 2022.

However, for both rain events, significant differences in $\delta^{18}O$ among all pre-event water sources were observed, except between total soil water and residential runoff, with the lowest mean values of $\delta^{18}O$ detected in rainwater and the highest mean values of $\delta^{18}O$ found in pre-event mobile soil water. The $\delta^{18}O$ varied within a narrower range across all pre-event water sources for the rain event in the drier and warmer 2022. The detected higher mean values of $\delta^{18}O$ in pre-event mobile soil water than in pre-event total soil water and groundwater can be attributed to the stronger evaporation occurring in mobile water holding in large pores (water held at suctions > -80 kPa) prior to rainfall (Sprenger et al., 2018; Zhao et al., 2013b). The observed lower mean values of $\delta^{18}O$ in groundwater than in both total and mobile soil water indicate that rainwater from the earlier events (not monitored) before the two events investigated in this study preferentially recharged the groundwater, probably through the macropores in the thin soil layer and the fractures in the underlying mudrock (Zhang et al., 2016; Zhao et al., 2013a; Zhao et al., 2016).

The $F_{max}(C1)/F_{max}(C2)$ ratios of total and mobile soil water exhibited similar variations. In contrast, the $\delta^{18}O$ value of the total soil water varied within a narrower range than that of the mobile soil water, indicating that the evaporation effect was more variable in the mobile soil water (Sprenger et al., 2018; Brooks et al., 2009; Goldsmith et al., 2012). In addition, the difference in $\delta^{18}O$ variation between total and mobile soil water was greater in the drier and warmer conditions in 2022. Both the $F_{max}(C1)/F_{max}(C2)$ ratio and $\delta^{18}O$ were more stable in the

total soil water than in the mobile soil water.

3.3. Differences in $F_{max}(C1)/F_{max}(C2)$ ratio and $\delta^{18}O$ among pre-event total soil waters of lands with different vegetation covers

The values of $F_{max}(C1)/F_{max}(C2)$ ratio and $\delta^{18}O$ in the pre-event total soil water of lands with different vegetation cover are shown in Fig. S2. Before both rain events, the highest mean values of $F_{max}(C1)/F_{max}(C2)$ ratio were detected in the soil water from grasslands and the lowest mean values of $F_{max}(C1)/F_{max}(C2)$ ratio were found in the soil water from paddy fields. The $F_{max}(C1)/F_{max}(C2)$ ratios in the soil water were significantly higher in grasslands and forestlands than in sloping farmlands, orchards, and paddy fields, where crop straws and fertilizers are often applied. The significantly lower $F_{max}(C1)/F_{max}(C2)$ ratios in the soil water of paddy fields than those of both sloping farmlands and orchards indicate that flooding may lead to a greater relative abundance of fulvic acid fluorophores (Li et al., 2013). The mean values of $F_{max}(C1)/F_{max}(C2)$ ratio in soil water varied in a slightly wider range (1.26–1.79) across different vegetation covers in the drier and warmer 2022.

However, for both rain events, the lowest mean values of $\delta^{18}O$ were detected in the pre-event soil water in the paddy fields, which can be attributed to their higher soil water storage under flooded conditions. Nevertheless, the differences in $\delta^{18}O$ in soil water among the vegetation cover types did not reach a significance level of 0.05.

The $F_{max}(C1)/F_{max}(C2)$ ratio showed a higher potential than $\delta^{18}O$ for distinguishing soil waters of lands under different vegetation cover types, despite the insignificant differences ($p > 0.05$) in $F_{max}(C1)/F_{max}(C2)$ ratio of soil water found between grasslands and forestlands, as well as between sloping farmlands and orchard lands. Similar distribution patterns of $F_{max}(C1)/F_{max}(C2)$ ratio in the soil water across different vegetation cover types were observed prior to the two rain events, reflecting the stable nature of $F_{max}(C1)/F_{max}(C2)$ ratio required for tracers.

3.4. Relationships between $F_{max}(C1)/F_{max}(C2)$ ratio and $\delta^{18}O$ in water sources and streamflow

Tracer value in a specific pre-event water source can show temporal/spatial variability (Birkel et al., 2020). The ^{18}O in soil water can be enriched with time and depth owing to evaporative fractionation (Zhao et al., 2016). The DOM fluorescence of soil water can vary with depth because of the increase in microbial-derived DOM and decrease in plant-derived DOM with depth (Hu et al., 2016; Ye et al., 2020). The results of linear regression analysis between $F_{max}(C1)/F_{max}(C2)$ ratio and $\delta^{18}O$ in rainwater and pre-event water sources are shown in Fig. S3.

A significant and positive relationship between $F_{max}(C1)/F_{max}(C2)$ ratio and $\delta^{18}O$ in groundwater was observed prior to the August 22, 2021 rain event but not before the June 26, 2022, rain event, implying that a higher spatial variation in recharging source composition of groundwater and poorer hydrologic connectivities among the monitoring wells could occur in a drier year. Significant linear $F_{max}(C1)/F_{max}(C2)$ ratio vs $\delta^{18}O$ regression equations ($p < 0.01$ or 0.05) were found for pre-event total soil waters under all different vegetation covers in the drier 2022, indicating that the $F_{max}(C1)/F_{max}(C2)$ ratio was as conservative as $\delta^{18}O$. Nevertheless, the relationships between $F_{max}(C1)/F_{max}(C2)$ ratio and $\delta^{18}O$ in residential runoff and soil waters of grassland and sloping farmland prior to the August 22, 2021, did not reach a significance level of 0.05, reflecting the greater temporal (runoff baseflow) or spatial variations (between pre-event soil waters of two replicate lands) in $F_{max}(C1)/F_{max}(C2)$ ratio. In both years, the relationships between $F_{max}(C1)/F_{max}(C2)$ ratio and $\delta^{18}O$ in pre-event soil waters of the forestland, orchard lands and paddy fields were significant ($p < 0.01$ or 0.05), reflecting that the conservative nature of $F_{max}(C1)/F_{max}(C2)$ was not affected by the inter-annual climatic changes.

The results of linear regression analysis between $F_{max}(C1)/F_{max}(C2)$ ratio and $\delta^{18}O$ of streamflow at four sampling locations were shown in Fig. S4. At the outlets of the Jieliu catchment (S_{JL}) and its three sub-catchments (S_F, S_R, and S_{AF}), significant linear relationships between $F_{max}(C1)/F_{max}(C2)$ ratio and $\delta^{18}O$ were observed during the heavier rain event in the wetter 2021, implying that the contributing sources water to streamflow might remain unchanged throughout the rain event. The linear relationships between $F_{max}(C1)/F_{max}(C2)$ ratio and $\delta^{18}O$ of streamflow at S_F and S_{AF} during the lighter rain event in the drier 2022 did not reach a significant level of 0.05, which can be attributed to the observed lower antecedent wetness in forest soil on steep slopes, as also reported previously (Wang et al., 2015). Source areas on slopes start to contribute to streamflow only after the soil moisture exceeds a storage threshold (Buttle et al., 2004). In contrast, a significant linear relationship between $F_{max}(C1)/F_{max}(C2)$ ratio and $\delta^{18}O$ was observed at S_{JL} during the June 26, 2022, rain event. Therefore, it can be inferred that the heterogeneity of water sources can be overcome by increasing the catchment size for monitoring through overlying land-use and topography effects. Similarly, positive and linear relationships between $F_{max}(C2)/F_{max}(C1)$ ratio and $\delta^{18}O$ were observed in surface runoff and fracture flow in a 0.15 ha sloping farmland plot located in the same catchment as this study (Xian et al., 2018). The significant linear relationships between $F_{max}(C1)/F_{max}(C2)$ ratio and $\delta^{18}O$ observed in the streamflow at the outlet of the Jieliu catchment for the two contrasting rain events indicate that the two tracers are identically conservative. Notably, higher p values of relationships between $F_{max}(C1)/F_{max}(C2)$ ratio and $\delta^{18}O$ were observed in the streamflow at all four sampling locations during the lighter rain event in the drier 2022, reflecting higher spatial (S_F, S_{AF}, and S_{JL}) or temporal (at S_R) variations in hydrologic connectivity between source areas and the stream. The capability of $F_{max}(C1)/F_{max}(C2)$ ratio to track the water sources of streamflow in a mixed land-use catchment may vary with climatic conditions.

3.5. Responses of streamflow discharge, $F_{max}(C1)/F_{max}(C2)$ ratio, and $\delta^{18}O$ to rain events

Temporal variations in the discharge, $F_{max}(C1)/F_{max}(C2)$ ratio, and $\delta^{18}O$ of streamflow at four locations in the Jieliu catchment in response to two rain events are shown in Fig. 3, and rainfall-induced streamflow depths are listed in Table 1.

During both rain events, the quickest response of streamflow discharge and the simultaneous occurrence of maximum discharge and maximum rainfall intensity (I_{max}) were observed at the outlet (S_R) of the residential sub-catchment which was dominated by an impermeable paved surface (e.g., concrete). During the August 22, 2021, rain event, the longest delay (45 min) of maximum discharge (relative to the occurrence of I_{max}) occurred at the outlet (S_{AF}) of the agro-forest sub-catchment and a 30 min delay of maximum discharge was observed at the outlet (S_{JL}) of the Jieliu catchment. During the June 26, 2022, rain event, the longest delay (1 h) of maximum discharge also occurred at S_{AF}, and a 45 min delay of maximum discharge at S_{JL} was observed. For the lighter rain event in 2022, delays in the maximum streamflow discharge at the outlets of the Jieliu catchment and its forest (S_F) and agro-forest sub-catchments were longer by the same magnitude (15 min).

The streamflow depths at the outlets of the catchment and its three sub-catchments accounted for much lower fractions of rainfall during the rain event in drier and warmer 2022, which can be attributed to the observed lower levels of both pre-event soil moisture and groundwater (data not shown). During both rain events, it is not surprising that the highest streamflow depth to rainfall amount ratios (0.31 and 0.10 on August 22, 2021, and June 26, 2022, respectively) were observed at S_R while the ratios at S_{JL} (0.16 and 0.06 on August 22, 2021, and June 26, 2022, respectively) were the highest among the other three sampling outlets.

Among four sampling locations, the $F_{max}(C1)/F_{max}(C2)$ ratio exhibited the highest values (2.25 ± 0.72 on August 22, 2021; 2.09 ±

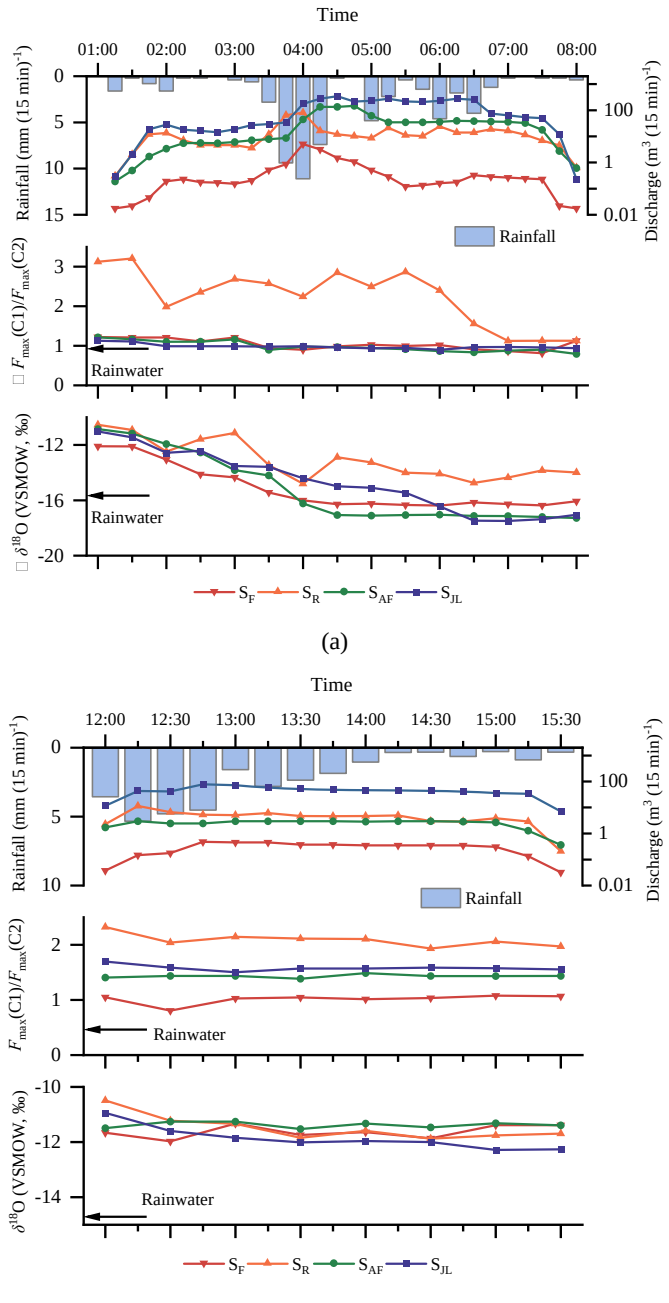

Fig. 3. Responses of discharge, $F_{max}(C1)/F_{max}(C2)$, and $\delta^{18}O$ of streamflow at the outlets of the Jieliu (S_{JL}) catchment and its nested forest (S_F), residential (S_R), and agro-forest (S_{AF}) sub-catchments to the August 22, 2021 (a) and June 26, 2022 (b) rain events.

0.12 on June 26, 2022) in residential runoff at S_R. This phenomenon may be attributed to the presence of abundant domestic sewage in the runoff, which is rich in microorganism originating from humic components and protein-like substances as well (Li et al., 2014). At the rising stage of the streamflow discharge, the $F_{max}(C1)/F_{max}(C2)$ ratio responded by varying magnitudes, with the strongest responses observed at the S_R for both rain events. At the receding stage, the $F_{max}(C1)/F_{max}(C2)$ ratios in streamflow rebound gradually by varying magnitudes but did not return to the levels of the first samples for both rain events. It should be noted that the $F_{max}(C1)/F_{max}(C2)$ ratio in the streamflow from drainage areas with different land-use compositions generally varied in distinct ranges during the June 26, 2022, rain event, indicating that the potential of $F_{max}(C1)/F_{max}(C2)$ ratio for tracing water sources under different land uses could be higher in a lighter rain event in a drier year.

For both rain events, the $\delta^{18}O$ values in the first rainfall generated streamflow samples collected at four sampling locations were much higher than those in rainwater samples, reflecting that pre-event water (s) with enriched $\delta^{18}O$ constituted varying proportions of streamflow. At the rising stage of streamflow hydrograph, the $\delta^{18}O$ generally decreased with increasing discharge, reflecting that the contribution of the low $\delta^{18}O$ rainwater to streamflow increased. At the receding stage, the $\delta^{18}O$ increased gradually but did not rebound to the levels of the first streamflow sample, implying that large portions of pre-event soil water (s) were displaced by rain event water.

Overall, the $F_{max}(C1)/F_{max}(C2)$ ratio, despite its gentler responses to rainfall compared to $\delta^{18}O$ (except its continuing dramatic decrease in the residential runoff during the late receding stage of the August 22, 2021, rain event, probably as a result of high proportion replacement of pre-event water by rainwater (Fig. S5)), appears to be a better tracer than $\delta^{18}O$ for distinguishing water sources under different land uses.

3.6. Comparison of hydrograph separation by $F_{max}(C1)/F_{max}(C2)$ ratio and $\delta^{18}O$ in a single land-use drainage area

The hydrograph separation results of streamflow at the outlet of the forest sub-catchment during two monitored rain events based on $F_{max}(C1)/F_{max}(C2)$ ratio and $\delta^{18}O$ data were shown in Figs. 4 and S5 and Table 2. The separation results based on $F_{max}(C1)/F_{max}(C2)$ ratio data showed that the estimated contributions of soil water to streamflow varied in the ranges of 25.5–75.5 % and 54.4–85.4 % during the August 22, 2021, and June 26, 2022, rain events, respectively. The contributions of soil water estimated from $\delta^{18}O$ data were found to vary in similar ranges during the August 22, 2021 (25.7–71.1 %) and June 26, 2022 (58.8–78.5 %) rain events as the ranges estimated from $F_{max}(C1)/F_{max}(C2)$ ratio data. The mean contribution of rainwater to streamflow during the August 22, 2021, rain event (56.0 % and 56.7 % estimated from $F_{max}(C1)/F_{max}(C2)$ ratio and $\delta^{18}O$ data, respectively) was much higher than that during the June 26, 2022, rain event (27.0 % and 27.6 % estimated from $F_{max}(C1)/F_{max}(C2)$ ratio and $\delta^{18}O$ data, respectively). No delay in the maximum rainwater contribution relative to the maximum streamflow discharge was observed for either rain events, indicating the dominance of piston flow in the generation of streamflow. Source apportion results, estimated from both $F_{max}(C1)/F_{max}(C2)$ ratio and $\delta^{18}O$, for streamflow (Figs. 4 and S5) and soil waters (Figs. S6 and

Table 1
Streamflow discharges at four locations in the Jieliu catchment during two rain events.

Rain event date	PD	Rain amount	Rain duration	I_{max}	Streamflow depth			
	(day)	(mm)	(h)	(mm (15 min)$^{-1}$)	(mm)			
					S_F	S_R	S_{AF}	S_{JL}
August 22, 2021	2	57.90	7.0	11.10	1.01	17.71	3.99	9.03
June 26, 2022	3	30.65	4.0	5.34	0.27	2.97	0.16	1.88

Notes: PD is preceding dry day; I_{max} is maximum rainfall intensity; flow depth was calculated by dividing cumulative discharge excluding the base flow discharge (if present) during each rain event by the projected drainage area.

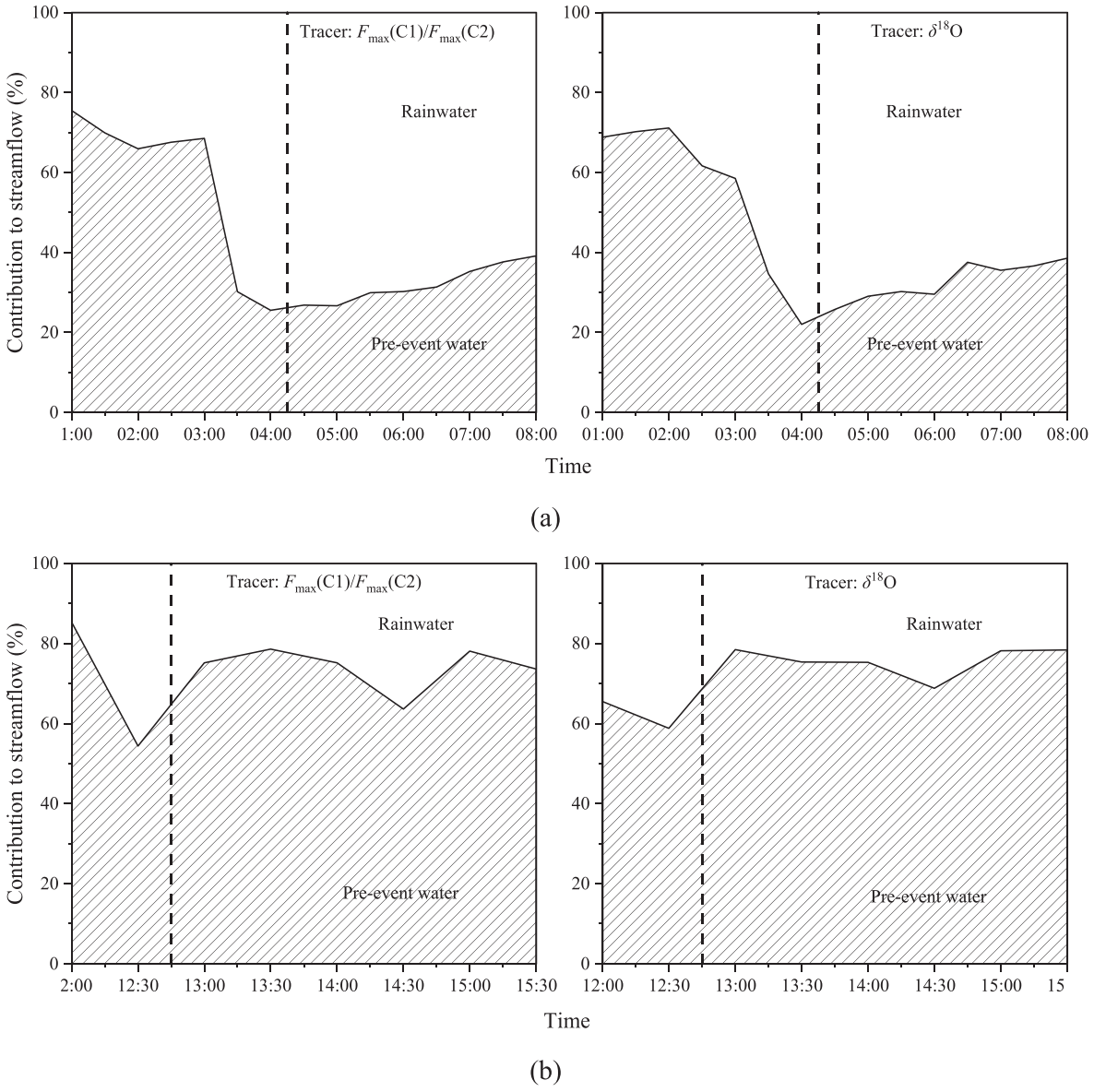

Fig. 4. Estimated proportions of rainwater and pre-event forest soil water in streamflow at the outlet of the forest sub-catchment (S_F) during the August 22, 2021 (a) and June 26, 2022 (b) rain events from F_{max}(C1)/F_{max}(C2) ratio data. The vertical dashed lines indicate the times of the streamflow peak discharges and separate the rising and receding stages. The intervals of water sampling and discharge measurement were 30 min and 15 min, respectively. Only the time differences between peak rain water contribution and peak discharge ≥30 min were regarded as valid differences.

S7) showed that rainwater could eventually replace a major portion of the water in the topsoil and small portions of the water in deeper soil layers and become the principal water source of streamflow during heavy rain events. Similarly, during a storm event, rainwater almost entirely replaced the pre-event water in the topsoil of sloping farmlands located in the same catchment as in the present study (Zhao et al., 2013b).

Statistical analysis showed that the hydrograph separation results based on F_{max}(C1)/F_{max}(C2) ratio data were satisfactorily consistent with those by δ^{18}O data, as indicated by the small RMSE values (4.4 % and 7.8 % for the August 22, 2021, and June 26, 2022, rain events, respectively) and the high R^2 values (0.948 and 0.629 for the August 22, 2021, and June 26, 2022, rain events, respectively) ($p < 0.05$). This validates the applicability of using F_{max}(C1)/F_{max}(C2) ratio data to identify the water sources of streamflow in a small forest catchment.

3.7. Application of F_{max}(C1)/F_{max}(C2) ratio to streamflow hydrograph separation in mixed land-use drainage areas

Given that the F_{max}(C1)/F_{max}(C2) ratio can distinguish more than two water sources of streamflow and appears to be conservative during the mixing of rainwater and pre-event water in various single land-use drainage areas (e.g., forest and sloping farmland), as indicated by the satisfactory result of comparison with δ^{18}O in this study and our previous study (Xian et al., 2018), it is plausible to assume that the F_{max}(C1)/F_{max}(C2) ratio is also applicable to the hydrograph separation of streamflow in mixed land-use drainage areas. The hydrograph separation results of the streamflow at the outlets of the Jieliu Catchment (S_{JL}) and its agro-forest sub-catchment (S_{AF}) under the two monitored rain events based on F_{max}(C1)/F_{max}(C2) ratio data are shown in Fig. 5 and Table 2. It should be noted that the inclusion of residential runoff baseflow at the S_R as an end-member of streamflow resulted in unacceptably high standard deviations of the hydrograph separation results with IsoSource. Therefore, residential runoff, given its very low

Table 2
Statistical and uncertainty results of water source proportions of streamflow at the outlets of the Jieliu (S_{JL}) catchment and its forest (S_F) and agro-forest (S_{AF}) sub-catchments estimated from F_{max}(C1)/F_{max}(C2) ratio data using the IsoSource model.

Rain event date	Outlet	Source water contribution to streamflow							
		Rainwater	Forest SW	Orchard SW	Sloping Farmland SW	Paddy SW	Grassland SW	Residential runoff	Groundwater
		- Mean ± SD -							
		- (uncertainty range) -							
		- % -							
August 22, 2021	S_F	56.0 ± 10.1 (NU)	44.0 ± 10.1 (NU)	NS	NS	NS	NS	NS	NS
	S_{AF}	36.5 ± 6.0 (13.4–17.1)	13.7 ± 1.6 (9.1–13.1)	NS	15.1 ± 2.8 (9.7–14.4)	23.4 ± 5.2 (16.3–19.3)	NS	NS	11.3 ± 3.9 (4.3–7.8)
	S_{JL}	25.3 ± 6.0 (10.5–16.7)	11.0 ± 0.5 (8.6–10.5)	14.1 ± 0.4 (7.9–11.7)	13.7 ± 0.9 (7.9–11.1)	17.2 ± 2.0 (9.8–15.8)	11.7 ± 1.0 (5.6–8.8)	NS	7.1 ± 2.8 (3.2–6.0)
June 26, 2022	S_F	27.0 ± 9.7 (NU)	73.0 ± 9.7 (NU)	NS	NS	NS	NS	NS	NS
	S_{AF}	15.6 ± 2.5 (15.6–16.2)	17.2 ± 1.3 (16.4–17.2)	NS	24.3 ± 3.5 (17.2–17.4)	33.0 ± 2.1 (17.4–17.6)	NS	NS	10.0 ± 4.1 (9.6–10.1)
	S_{JL}	11.1 ± 1.5 (5.4–6.9)	13.6 ± 1.1 (7.6–11.4)	22.5 ± 1.7 (8.4–13.6)	23.4 ± 0.8 (8.7–11.9)	10.0 ± 0.2 (5.6–7.8)	13.7 ± 1.4 (5.7–9.7)	NS	5.8 ± 2.0 (2.4–3.9)

Notes: SW is total soil water; SD is standard deviation; NU means that no uncertainty was obtained for the two end-member analysis at S_F; NS means there is no feasible solution if this water source is included in modeling; mean and standard deviation of each water source's contribution to streamflow at the outlet of a particular drainage area during a rain event were calculated from the mean values of source proportions estimated for each stream sample.

discharges (Fig. 3 and Table 1), was excluded as a pre-event water source for streamflow at S_{JL} in hydrograph separation.

The total contributions of all pre-event water sources to streamflow at S_{AF} varied in the ranges of 51.6–85.5 % and 81.9–88.3 % during the August 22, 2021, and June 26, 2022, rain events, respectively. The mean contribution of rainwater to streamflow at S_{AF} during the heavier rain event on August 22, 2021 (36.5 %) was much higher than that during the lighter rain event on June 26, 2022 (15.6 %). The maximum contribution of rainwater to streamflow at S_{AF} occurred 45 min earlier than the maximum streamflow discharge during the August 22, 2021, rain event, implying the preferential movement of rainwater through large soil pores and mudrock fractures, as well as overland flow to the stream, particularly on sloping farmlands. This explanation is supported by the stronger preferential flow on sloping farmland than on forestland observed at the same site in previous studies (Wang et al., 2013; Zhao et al., 2013a) and the finding at other sites that rainwater could be the main component of the streamflow during high rainfall intensity events (Genereux and Hooper, 1998; McGlynn and McDonnell, 2003). Nevertheless, the maximum contribution of rainwater to the streamflow at S_{AF} occurred at the same time as the maximum streamflow discharge during the lighter rain event on June 26, 2022.

The total contributions of all pre-event water sources to streamflow at S_{JL} varied in narrower ranges (67.4–85.6 % and 85.5–89.8 % during the August 22, 2021, and June 26, 2022, rain events, respectively) than those at S_{AF}. The mean contributions of rainwater to streamflow at S_{JL} (25.3 % and 11.1 % during the August 22, 2021, and June 26, 2022, rain events, respectively) were much lower than those at S_{AF}, which can be attributed to the involvement of two more vegetation cover types (orchard land and grassland) in the highland area. The soils of orchards and grassland are better structured and exhibit higher water storage capacities than the macroporous soils of sloping farmlands and forestlands (Wang et al., 2013; Zhao et al., 2013a). Therefore, orchard land and grassland are two important water sources for the streamflow at the outlet of the Jieliu Catchment. The maximum contribution of rainwater to streamflow at S_{JL} occurred 1.5 h after the maximum streamflow discharge during the heavier rain event on August 22, 2021, reflecting the increased dominance of piston flow in the movement of pre-event soil water and, consequently, a longer time for rainwater to enter the stream. In contrast, no delay in the maximum rainwater contribution relative to the maximum streamflow discharge was observed at S_{JL} during the lighter rain event on June 26, 2022. This result agrees with a previous finding that high pre-event soil water content and high rain intensity favor the occurrence of piston flow (Zhao et al., 2013b).

Among the various pre-event water sources, the greatest mean contribution (23.4 % and 33.0 % during the August 22, 2021, and June 26, 2022, rain events, respectively) to streamflow at S_{AF} came from the soil water of paddy fields in the valley area during both rain events. The contribution of soil water from paddy fields to streamflow is more dominant during the lighter rain event in 2022. The greatest mean contribution (17.2 %) of pre-event water to streamflow at S_{JL} on August 22, 2021 also came from the soil water of the paddy fields, particularly during the rising stage of the streamflow hydrograph. Nevertheless, the soil water of sloping farmlands, which accounted for the highest proportion of the total area of the Jieliu Catchment, made the greatest mean contribution to the streamflow at S_{JL} during lighter rain in 2022. For both rain events, the soil waters of the sloping farmland and orchard land were the second-largest contributor to streamflow at S_{AF} and S_{JL}, respectively (Table 2).

4. Discussion

4.1. Specificity of F_{max}(C1)/F_{max}(C2) ratio in water sources

Significant differences were observed in the ratio of F_{max} of the two conservative DOM components (i.e., C1and C2) among water sources, including rainwater and pre-event waters (total soil water, groundwater and residential runoff) (Fig. S1), indicated the potential of using the abundance ratio of conservative DOM components for the separation of water sources under different land uses. However, the differences in F_{max} (C1)/F_{max} (C2) ratios among the pre-event soil waters under different vegetation cover types did not always reach a significance level of 0.05 (Fig. S2), which may be partly responsible for the uncertainties associated with the streamflow hydrograph separation results estimated from F_{max} (C1)/F_{max} (C2) ratio data (Table 2). In addition, the lower p values of F_{max}(C1)/F_{max}(C2) ratio vs $\delta^{18}O$ regressions for water sources (except the groundwater and paddy field, which have high water storage and are saturated) observed for the lighter rain event in 2022 indicate that values of both tracers in each water source were highly subject to evaporation process and thus exhibited higher capabilities for tracing water source(s) in a drier and warmer year (Fig. S3).

4.2. Scale of conservative mixing of F_{max}(C1)/F_{max}(C2) ratio

The most conservative tracer of water source is the isotopic signature

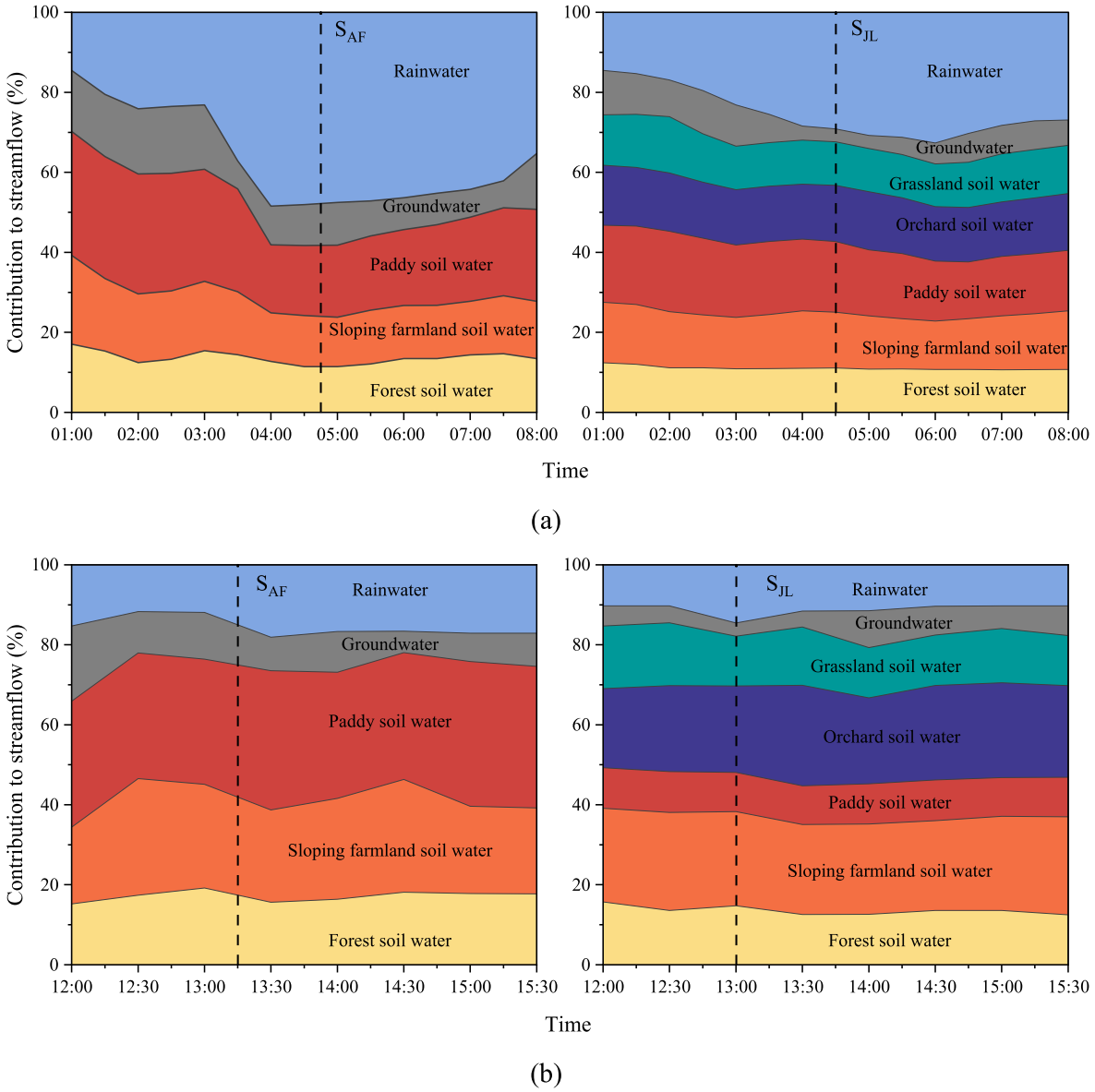

Fig. 5. Estimated proportions of rainwater and pre-event waters in the streamflow at the outlets of the Jieliu catchment (S_{JL}) and its agro-forest sub-catchment (S_{AF}) during the August 22, 2021 (a) and June 26, 2022 (b) rain events from $F_{max}(C1)/F_{max}(C2)$ ratio data. The vertical dashed lines indicate the times of the peak streamflow discharges and separate the rising and receding stages. The intervals of water sampling and discharge measurement were 30 min and 15 min, respectively. Only the time differences between peak rain water contribution and peak discharge ≥30 min were regarded as valid differences.

of the water itself, which allows for the precise separation of event and pre-event water at multiple spatial and temporal scales (Jasechko et al., 2016; Kirchner, 2016; McDonnell, 1990; Zhao et al., 2013a, 2013b). Nevertheless, the observed much poorer specificity of $\delta^{18}O$ in different pre-event water sources than that of DOM $F_{max}(C1)/F_{max}(C2)$ ratio in this study precludes the applicability of $\delta^{18}O$ to tracking more than two water sources (e.g., rain event water and ≥ 2 pre-event waters) (Figs. S1 and S2). Previously reported conservative mixing at large river confluences highlighted the potential of DOM as a tracer for water source discrimination over short distances (Xue et al., 2022). The higher p values of $F_{max}(C1)/F_{max}(C2)$ ratio vs $\delta^{18}O$ regressions for streamflow observed at the Jieliu catchment and its agro-forest sub-catchment (both with mixed land uses) during the lighter rain event in the drier and warmer 2022 (Fig. S4) resulted from the greater total contributions of pre-event water sources (mean: 89.0 % and 84.5 %, respectively; Table 2) and the mixing of pre-event water sources having more distinctive ranges of $F_{max}(C1)/F_{max}(C2)$ ratio but similar ranges of $\delta^{18}O$ (Fig. S3). The observed more significant linear relationships ($p = 0.001$ or $p < 0.001$) between $F_{max}(C1)/F_{max}(C2)$ ratio and $\delta^{18}O$ in the streamflow at multiple spatial scales (i.e., S_F, S_{AF}, and S_{JL}) during the heavier rain event in the wet 2021 was not surprising and can be attributed to the much higher contributions of rainwater to streamflow (Fig. S4; Table 2).

4.3. Hydrograph separation based on $F_{max}(C1)/F_{max}(C2)$ ratio

Land use can affect both the quantity (discharge and dynamics) and the quality of streamflow (Klaus and McDonnell, 2013). Isotope-based hydrograph separation may be limited in enabling new process insights (e.g., regarding temporal-spatial variations in the contributions of soil waters from different land uses to streamflow). The $F_{max}(C1)/F_{max}(C2)$ ratio, as a DOM composition parameter showing a more conservative nature and higher specificity than dissolved organic carbon concentration, can be used in the hydrograph separation of streamflow/

runoff not only at the plot scale (Xian et al., 2018) but also at the catchment scale (as shown in this study). Moreover, because the two humic components (C1 and C2) of DOM are much more conservative than the protein-like component during their transport by water, they can also be used to identify the water sources of rivers, shallow groundwater, and deeper aquifers, and to examine water exchanges among these water bodies (Hu et al., 2016).

As a novel tracer, the F_{max}(C1)/F_{max}(C2) ratio can be used to analyze temporal variations in the proportions of rainwater and various pre-event waters (e.g., soil water under different vegetation covers, residential runoff, and groundwater). Uncertainties associated with the hydrograph separation results (Table 2) obtained using F_{max}(C1)/F_{max}(C2) ratio as the only tracer can be partially attributed to the observed insignificant ($p > 0.05$) differences in F_{max}(C1)/F_{max}(C2) ratio between some pre-event soil water end-members (i.e., between grasslands and forestlands and between sloping farmlands and orchards), particularly in drier 2022 (Fig. S2). Developing more tracers with distinct properties and using multiple tracers with high specificity among water sources can reduce uncertainty and improve the process understanding across catchments (Abbott et al., 2016).

Key factors affecting streamflow composition include land use, landscape (e.g., topography, geology, and vegetation cover), antecedent soil moisture conditions, rainfall characteristics and catchment size (Klaus and McDonnell, 2013). The greater dominance of the contribution of paddy fields to the streamflow at the outlet of the agro-forest sub-catchment observed during the lighter rain event in drier 2022 can be attributed to the lower antecedent soil water contents detected in farmlands (data not shown) in drier 2022. The pre-event soil water in the paddy fields flowed into ditches connected to the main stream through piston infiltration and subsequent lateral seepage above the impermeable soil layer, as observed in the field. Forestlands accounted for the second largest portion of the Jieliu catchment's total area; however, the contribution of their soil water to streamflow was disproportionally low, which could be attributed to the lower water storage of thinner forest soil layer (mostly <50 cm) distributed largely on relatively steep (10.0°–21.5°) slopes. The greater total contribution (55.9 %) of soil waters from sloping farmlands, orchards, and paddy fields observed at the outlet of the Jieliu catchment during the June 26, 2022, rain event might have led to a greater loading of pollutants (various agrochemicals applied) to the stream.

4.4. Limitations and future research needs

This study has two limitations. First, only two rain events in two contrasting years were investigated, which does not allow the evaluation of the applicability of F_{max}(C1)/F_{max}(C2) ratio to hydrograph separation of streamflow in response to different rain characteristics in the same year with similar climatic contexts in summer. Second, the sizes of the study catchment and its nested sub-catchments area were relatively small, and an ideal comparison across hydrologically independent catchments of different sizes and land uses/vegetation covers was not made for a more systematic and extensive validation. Despite these limitations, the findings of this study provide a novel, cost-effective and promising approach for quantitatively identifying more than two streamflow water sources based on distinct signatures of conservative fluorescent DOM components that originate from diverse organic materials applied/discharged to lands and are subject to biogeochemical transformation (Graeber et al., 2015; Park et al., 2018).

Novel tracers can open new possibilities for more precise water resource management and implementation of better targeted water pollution control in mixed land-use mosaic catchments. In a broad set of anthropogenic, topographic, and climatic contexts, the combined use of multiple tracers of different types (e.g., water isotopes and conservative solutes resulting from various natural biogeochemical processes or anthropogenic activities) can lead to more reliable hydrograph separation results (Bauer et al., 2001).

A number of questions remain to be answered by future studies on the water source tracing method using the F_{max}(C1)/F_{max}(C2) ratio of DOM: First, do the F_{max}(C1)/F_{max}(C2) ratios of water sources remain constant during the course of a rain event? Second, what is the significance of temporal and spatial variations in the F_{max}(C1)/F_{max}(C2) ratio across sampling locations for each land-use/vegetation cover type in a mixed land use catchment of a larger size? Third, in hilly catchments with a thin soil layer, how do we consider the potential effect of spatial variations in soil thickness (within each land-use type and across different land types) on streamflow hydrograph separation using the F_{max}(C1)/F_{max}(C2) ratio? Fourth, are there any other land-use indices that can be used together with the F_{max}(C1)/F_{max}(C2) ratio to reduce the uncertainty of hydrograph separation results?

Knowledge of water sources and their flow pathways to streams is essential for effective pollution control in a mixed land-use catchment (Lv et al., 2018). There is a clear need to develop a targeted sampling strategy for crossing the DOM F_{max}(C1)/F_{max}(C2) ratio with other tracers to determine both the water source and flow path.

5. Conclusions

Various pollutants are discharged into streams via hydrological process as a result of diverse land uses, and there is clearly a need to develop new tools for tracing water sources in mixed-land-use catchments. In this study, the ratio of F_{max} of two relatively stable DOM components in environmental media is proposed as a novel water tracer. The applicability of using F_{max}(C1)/F_{max}(C2) ratio for hydrography separation was validated in a forest sub-catchment of the Jieliu catchment by comparing with the hydrography separation results based on $\delta^{18}O$ data during two rain events. The water source tracking method using the F_{max}(C1)/F_{max}(C2) ratio was then applied to an agro-forest sub-catchment and the entire catchment (both with multiple land uses/vegetation covers). Among the pre-event water sources, soil water from paddy fields made the highest contribution to streamflow at the outlet of the agro-forest sub-catchment. At the outlet of the Jieliu Catchment, sloping farmlands were the greatest contributors of pre-event water during the lighter rain event in drier 2022, whereas paddy fields were the greatest contributors of pre-event water to streamflow during the heavier rain event in wetter 2021. Hydrograph separation results based on F_{max}(C1)/F_{max}(C2) ratio data can be used to support the optimization of water resource management and the estimation of pollutant loadings from major water sources to streams at the catchment scale.

CRediT authorship contribution statement

Zhi-Xiang Sun: Investigation, Writing – original draft. **Jun-Fang Cui:** Resources, Funding acquisition, Supervision. **Jian-Hua Cheng:** Funding acquisition, Methodology. **Xiang-Yu Tang:** Conceptualization, Supervision, Writing – review & editing, Funding acquisition.

Declaration of competing interest

The authors declare that they have no known competing financial interests or personal relationships that could have appeared to influence the work reported in this paper.

Data availability

Data will be made available on request.

Acknowledgements

This study was supported by the Zhejiang Provincial Natural Science Foundation of China (Grant No. LD21D010001), the Sichuan Provincial Natural Science Foundation of China (Grant No. 2022NSFSC0102), the

National Natural Science Foundation of China (Grant Nos. 42177379 and 42007361), and the ZAFU Scientific Research Development Foundation (Grant Nos. 2020FR040 and 2021LFR045).

Appendix A. Supplementary data

Supplementary data to this article can be found online at https://doi.org/10.1016/j.scitotenv.2023.168800.

References

Abbott, B.W., Baranov, V., Mendoza-Lera, C., Nikolakopoulou, M., Harjung, A., Kolbe, T., Balasubramanian, M.N., Vaessen, T.N., Ciocca, F., Campeau, A., Wallin, M.B., Romeijn, P., Antonelli, M., Goncalves, J., Datry, T., Laverman, A.M., de Dreuzy, J.R., Hannah, D.M., Krause, S., Oldham, C., Pinay, G., 2016. Using multi-tracer inference to move beyond single-catchment ecohydrology. Earth Sci. Rev. 160, 19–42.

Bauer, S., Fulda, C., Schäfer, W., 2001. A multi-tracer study in a shallow aquifer using age dating tracers ^{3}H, ^{85}Kr, CFC-113 and SF6 — indication for retarded transport of CFC-113. J. Hydrol. 248 (1–4), 14–34.

Begum, M.S., Park, H.Y., Shin, H.S., Lee, B.J., Hur, J., 2023. Separately tracking the sources of hydrophobic and hydrophilic dissolved organic matter during a storm event in an agricultural watershed. Sci. Total Environ. 873, 162347.

Birkel, C., Correa-Barahona, A., Martinez-Martinez, M., Granados-Bolanos, S., Venegas-Cordero, N., Gutierrez-Garcia, K., Blanco-Ramirez, S., Quesada-Mora, R., Solano-Rivera, V., Mussio-Mora, J., Chavarria-Palma, A., Vargas-Arias, K., Moore, G.W., Duran-Quesada, A.M., Vasquez-Morera, J., Soulsby, C., Tetzlaff, D., Espinoza-Cisneros, E., Sanchez-Murillo, R., 2020. Headwaters drive streamflow and lowland tracer export in a large-scale humid tropical catchment. Hydrol. Process. 34 (18), 3824–3841.

Brooks, J.R., Barnard, H.R., Coulombe, R., McDonnell, J.J., 2009. Ecohydrologic separation of water between trees and streams in a Mediterranean climate. Nat. Geosci. 3 (2), 100–104.

Buerge, I.J., Poiger, T., Müller, M.D., Buser, H.R., 2003. Caffeine, an anthropogenic marker for wastewater contamination of surface waters. Environ. Sci. Technol. 37 (4), 691–700.

Buerge, I.J., Buser, H.R., Kahle, M., Mueller, M.D., Poiger, T., 2009. Ubiquitous occurrence of the artificial sweetener acesulfame in the aquatic environment: an ideal chemical marker of domestic wastewater in groundwater. Environ. Sci. Technol. 43 (12), 4381–4385.

Burns, M.A., Barnard, H.R., Gabor, R.S., Mcknight, D.M., Brooks, P.D., 2016. Dissolved organic matter transport reflects hillslope to stream connectivity during snowmelt in a montane catchment. Water Resour. Res. 52 (6), 4905–4923.

Buttle, J.M., Dillon, P.J., Eerkes, G.R., 2004. Hydrologic coupling of slopes, riparian zones and streams: an example from the Canadian Shield. J. Hydrol. 287 (1–4), 161–177.

Cory, R.M., Kaplan, L.A., 2012. Biological lability of stream water fluorescent dissolved organic matter. Limnol. Oceanogr. 57 (5), 1347–1360.

Cotrufo, M.F., Haddix, M.L., Kroeger, M.E., Stewart, C.E., 2022. The role of plant input physical-chemical properties, and microbial and soil chemical diversity on the formation of particulate and mineral-associated organic matter. Soil Biol. Biochem. 168, 108648.

Fellman, J.B., Hood, E., Spencer, R.G.M., 2010. Fluorescence spectroscopy opens new windows into dissolved organic matter dynamics in freshwater ecosystems: a review. Limnol. Oceanogr. 55 (6), 2452–2462.

Genereux, D.P., Hooper, R.P., 1998. Oxygen and hydrogen isotopes in rainfall-runoff studies. In: Kendall, C., McDonnell, J.J. (Eds.), Isotope Tracers in Catchment Hydrology. Elsevier Science Limited, Amsterdam, pp. 319–346.

Goldsmith, G.R., Muñoz-Villers, L.E., Holwerda, F., McDonnell, J.J., Asbjornsen, H., Dawson, T.E., 2012. Stable isotopes reveal linkages among ecohydrological processes in a seasonally dry tropical montane cloud forest. Ecohydrology 5 (6), 779–790.

Graeber, D., Boechat, I.G., Encina-Montoya, F., Esse, C., Gelbrecht, J., Goyenola, G., Gucker, B., Heinz, M., Kronvang, B., Meerhoff, M., Nimptsch, J., Pusch, M.T., Silva, R.C., von Schiller, D., Zwirnmann, E., 2015. Global effects of agriculture on fluvial dissolved organic matter. Sci. Rep. 5, 16328.

Hiriart-Baer, V.P., Binding, C., Howell, T.E., 2013. Dissolved organic matter quantity and quality in Lake Simcoe compared to two other large lakes in southern Ontario. Inland Waters 3 (2), 139–152.

Hu, Y., Lu, Y.H., Edmonds, J.W., Liu, C., Wang, S., Das, O., Liu, J., Zheng, C.M., 2016. Hydrological and land use control of watershed exports of dissolved organic matter in a large arid river basin in northwestern China. J. Geophys. Res. Biogeosci. 121 (2), 466–478.

Jasechko, S., Kirchner, J.W., Welker, J.M., McDonnell, J.J., 2016. Substantial proportion of global streamflow less than three months old. Nat. Geosci. 9 (2), 126–129.

Kirchner, J.W., 2016. Aggregation in environmental systems – part 1: seasonal tracer cycles quantify young water fractions, but not mean transit times, in spatially heterogeneous catchments. Hydrol. Earth Syst. Sci. 20 (1), 279–297.

Klaus, J., McDonnell, J.J., 2013. Hydrograph separation using stable isotopes: review and evaluation. J. Hydrol. 505, 47–64.

Kothawala, D.N., Stedmon, C.A., Muller, R.A., Weyhenmeyer, G.A., Kohler, S.J., Tranvik, L.J., 2014. Controls of dissolved organic matter quality: evidence from a large-scale boreal lake survey. Glob. Chang. Biol. 20 (4), 1101–1114.

Landon, M.K., Delin, G.N., Komor, S.C., Regan, C.P., 1999. Comparison of the stable-isotopic composition of soil water collected from suction lysimeters, wick samplers, and cores in a sandy unsaturated zone. J. Hydrol. 224 (1–2), 45–54.

Li, M.T., Zhao, L.P., Zhang, J.J., 2013. Effect of temperature, pH and salt on fluorescent quality of water extractable organic matter in black soil. J. Integr. Agric. 12 (7), 1251–1257.

Li, W.T., Chen, S.Y., Xu, Z.X., Li, Y., Shuang, C.D., Li, A.M., 2014. Characterization of dissolved organic matter in municipal wastewater using fluorescence PARAFAC analysis and chromatography multi-excitation/emission scan: a comparative study. Environ. Sci. Technol. 48 (5), 2603–2609.

Liu, H.Y., Guan, Z., Cheng, J.H., Tang, X.Y., Xian, Q.S., 2022. Ambient temperature modulates dissipation and redistribution of chlorpyrifos and 3,5,6-trichloro-2-pyridinol in paddy field. Soil Sediment Contam. 31 (5), 533–555.

Lubick, N., 2009. Artificial sweetener makes ideal tracer. Environ. Sci. Technol. 43 (12), 4220.

Lv, Y., Gao, L., Geris, J., Verrot, L., Peng, X., 2018. Assessment of water sources and their contributions to streamflow by end-member mixing analysis in a subtropical mixed agricultural catchment. Agric. Water Manag. 203, 411–422.

McDonnell, J.J., 1990. A rationale for old water discharge through macropores in a steep, humid catchment. Water Resour. Res. 26 (11), 2821–2832.

McGlynn, B.L., McDonnell, J.J., 2003. Quantifying the relative contributions of riparian and hillslope zones to catchment runoff. Water Resour. Res. 39 (11), 1310.

Murphy, K.R., Stedmon, C.A., Graeber, D., Bro, R., 2013. Fluorescence spectroscopy and multi-way techniques. PARAFAC. Anal. Methods 5 (23), 6557–6566.

Park, J.H., Nayna, O.K., Begum, M.S., Chea, E., Hartmann, J., Keil, R.G., Kumar, S., Lu, X., Ran, L., Richey, J.E., Sarma, V.V.S.S., Tareq, S.M., Do Thi, X., Yu, R., 2018. Reviews and syntheses: anthropogenic perturbations to carbon fluxes in Asian river systems - concepts, emerging trends, and research challenges. Biogeosciences 15 (9), 3049–3069.

Phillips, D.L., Gregg, J.W., 2001. Uncertainty in source partitioning using stable isotopes. Oecologia 127 (2), 171–179.

Phillips, D.L., Gregg, J.W., 2003. Source partitioning using stable isotopes: coping with too many sources. Oecologia 136, 261–269.

Quiers, M., Batiot-Guilhe, C., Bicalho, C.C., Perrette, Y., Seidel, J.L., Exter, S.V., 2013. Characterisation of rapid infiltration flows and vulnerability in a karst aquifer using a decomposed fluorescence signal of dissolved organic matter. Environ. Earth Sci. 71 (2), 553–561.

Ramón, J., Correa, A., Timbe, E., Mosquera, G.M., Mora, E., Crespo, P., 2021. Do mixing models with different input requirement yield similar streamflow source contributions? Case study: a tropical montane catchment. Hydrol. Process. 35 (6), e14209.

Riml, J., Worman, A., Kunkel, U., Radke, M., 2013. Evaluating the fate of six common pharmaceuticals using a reactive transport model: insights from a stream tracer test. Sci. Total Environ. 458, 344–354.

Sprenger, M., Tetzlaff, D., Buttle, J., Laudon, H., Leistert, H., Mitchell, C.P.J., Snelgrove, J., Weiler, M., Soulsby, C., 2018. Measuring and modeling stable isotopes of mobile and bulk soil water. Vadose Zone J. 17 (1), 170149.

Stedmon, C.A., Markager, S., 2003. Behaviour of the optical properties of coloured dissolved organic matter under conservative mixing. Estuar. Coast. Shelf Sci. 57 (5–6), 973–979.

Stedmon, C.A., Markager, S., 2005. Resolving the variability in dissolved organic matter fluorescence in a temperate estuary and its catchment using PARAFAC analysis. Limnol. Oceanogr. 50 (2), 686–697.

Stewart, B., Shanley, J.B., Kirchner, J.W., Norris, D., Adler, T., Bristol, C., Harpold, A.A., Perdrial, J.N., Rizzo, D.M., Sterle, G., Underwood, K.L., Wen, H., Li, L., 2022. Streams as mirrors: reading subsurface water chemistry from stream chemistry. Water Resour. Res. 58 (1), e2021WR029931.

Voss, B.M., Peucker-Ehrenbrink, B., Eglinton, T.I., Spencer, R.G.M., Bulygina, E., Galy, V., Lamborg, C.H., Gangulii, P.M., Montlucon, D.B., Marsh, S., Gillies, S.L., Fanslau, J., Epp, A., Luymes, R., 2015. Seasonal hydrology drives rapid shifts in the flux and composition of dissolved and particulate organic carbon and major and trace ions in the Fraser River. Can. Biogeosci. 12 (19), 5597–5618.

Wang, Y.Q., Shao, M.A., Liu, Z.P., 2013. Vertical distribution and influencing factors of soil water content within 21-m profile on the Chinese Loess Plateau. Geoderma 193, 300–310.

Wang, H.L., Tang, X.Y., Zhang, W., Song, S.B., McKenzie, B.M., 2015. Within-year changes in hydraulic properties of a shallow entisol in farmland and forestland. Vadose Zone J. 14 (7) https://doi.org/10.2136/vzj2014.11.0163.

West, A.G., Patrickson, S.J., Ehleringer, J.R., 2006. Water extraction times for plant and soil materials used in stable isotope analysis. Rapid Commun. Mass Spectrom. 20 (8), 1317–1321.

Wickland, K.P., Aiken, G.R., Butler, K., Dornblaser, M.M., Spencer, R.G.M., Striegl, R.G., 2012. Biodegradability of dissolved organic carbon in the Yukon River and its tributaries: seasonality and importance of inorganic nitrogen. Global Biogeochem. Cycl. 26, Gb0e03.

Williams, C.J., Yamashita, Y., Wilson, H.F., Jaffe, R., Xenopoulos, M.A., 2010. Unraveling the role of land use and microbial activity in shaping dissolved organic matter characteristics in stream ecosystems. Limnol. Oceanogr. 55 (3), 1159–1171.

Xian, Q.S., Li, P.H., Liu, C., Cui, J.F., Guan, Z., Tang, X.Y., 2018. Concentration and spectroscopic characteristics of DOM in surface runoff and fracture flow in a cropland plot of a loamy soil. Sci. Total Environ. 622, 385–393.

Xiao, X., Zhang, X.P., Shi, X.N., Yu, Z.L., Liu, K.S., Liu, Z., 2023. Identifying river water sources using end-member mixing analysis in a subtropical monsoon basin China. Hydrol. Process. 37 (2), e14824.

Xue, J.P., Cuss, C.W., Noernberg, T., Javed, M.B., Chen, N., Pelletier, R., Wang, Y., Shotyk, W., 2022. Size and optical properties of dissolved organic matter in large

boreal rivers during mixing: implications for carbon transport and source discrimination. J. Hydrol. Reg. Stud. 40, 101033.
Ye, Q., Wang, Y.H., Zhang, Z.T., Huang, W.L., Li, L.P., Li, J., Liu, J., Zheng, Y., Mo, J.M., Zhang, W., Wang, J.J., 2020. Dissolved organic matter characteristics in soils of tropical legume and non-legume tree plantations. Soil Boil. Biochem. 148, 107880.
Zhang, W., 2015. Hydrological Processes and Colloid Transport in the Sloping Farmland of Purple Soil. Institute of Mountain Hazards and Environment, UCAS, Chengdu (PhD Dissertation).
Zhang, W., Tang, X.Y., Xian, Q.S., Weisbrod, N., Yang, J.E., Wang, H.L., 2016. A field study of colloid transport in surface and subsurface flows. J. Hydrol. 542, 101–114.
Zhang, W., Cheng, J.H., Xian, Q.S., Cui, J.F., Tang, X.Y., Wang, G.X., 2019. Dynamics and sources of colloids in shallow groundwater in lowland wells and fracture flow in sloping farmland. Water Res. 156, 252–263.
Zhao, L., Du, C.C., Zhang, Q., Sun, C., Wang, S.D., Luo, S.H., 2020. The ultraviolet-visible absorbance and fluorescence characterization of dissolved organic matter derived from the leaf litter of *Populus simonii*, *Artemisia desertorum*, *Salix cheilophila*, and *Populus tomentosa*. Environ. Sci. Pollut. Res. 27 (29), 36439–36449.
Zhao, P., Tang, X.Y., Zhao, P., Wang, C., Tang, J.L., 2013a. Tracing water flow from sloping farmland to streams using oxygen-18 isotope to study a small agricultural catchment in southwest China. Soil Tillage Res. 134, 180–194.
Zhao, P., Tang, X.Y., Zhao, P., Wang, C., Tang, J.L., 2013b. Identifying the water source for subsurface flow with deuterium and oxygen-18 isotopes of soil water collected from tension lysimeters and cores. J. Hydrol. 503, 1–10.
Zhao, P., Tang, X.Y., Zhao, P., Zhang, W., Tang, J.L., 2016. Mixing of event and pre-event water in a shallow Entisol in sloping farmland based on isotopic and hydrometric measurements. SW China. Hydrol. Process. 30 (19), 3478–3493.